Finite-difference model for one-dimensional electro-osmotic consolidation

Yadong Zhou[1], An Deng[2*], Can Wang[2]

1. Geotechnical Research Institute, MOE Key Laboratory for Geomechanics and Embankment Engineering, Hohai University, Nanjing, Jiangsu 210098, China
2. School of Civil, Environmental & Mining Engineering, IMER, The University of Adelaide, Adelaide, SA 5005, Australia.

* Corresponding author. E-mail: an.deng@adelaide.edu.au. Tel: +61 8 83132830. Fax: +61 8 83134359

Small strain consolidation theories treat soil properties as being constant and uniform in the course of consolidation, which is not true in the case of electro-osmosis-induced consolidation practices. Electro-osmotic consolidation leads to large strain, which physically and electro-chemically affects to a non-negligible extent the nonlinear changes of the soil properties. For the nonlinear changes, iterative computations provide a mathematical approximation of the soil consolidation when the time steps and spatial geometry are intensively meshed. In this context, this paper presents a finite-difference model, EC1, for one-dimensional electro-osmotic consolidation, and this model is developed based on a fixed Eulerian co-ordinate system and uses a piecewise linear approximation. The model is able to account for the large-strain-induced nonlinear changes of the physical and electro-chemical properties in a compressible mass subjected to electro-osmotic consolidation and to predict the consolidation characteristics of the compressible mass. EC1 is verified against exact analytical solutions and test results obtained from an experimental program. Example problems are illustrated with respect to the numerical solutions of large-strain electro-osmotic consolidation.

Key words: electro-osmosis, consolidation, large strain, non-linear, electrical potential, pore pressure

1. INTRODUCTION

Electro-osmosis is a process enabling the flow of pore fluid in a soil mass in the direction toward a negative electrode (cathode) in response to a voltage gradient (electrical field or potential difference) of direct current that is applied between the cathode and a positive electrode (anode). The cathode and anode are installed in pairs in the soil mass, between which electrical current is transmitted primarily by the movement of ions through the pore fluid. The capacity of electro-osmosis is employed in many geotechnical and geoenvironmental practices, such as soil remediation, site reclamation and ground dewatering, where clays or other very low permeability materials are intensively deposited and the uses of conventional soil treatment technology are less efficient. Though the liquid and solid phases are taken to be incompressible, the consolidation induced by electro-osmosis may subject the soil skeleton to significant compression for high moisture content fine-grained soils, e.g., newly reclaimed or dredged coastal sediments, municipal sludge and industry solid-liquid mixed disposals. That is, the soil properties undergo changes under electro-osmotic consolidation, which has been noted in many previous experiments[1-4]. The changes may be significant and non-negligible, so small strain electro-osmotic consolidation theories[5-7], which usually assume that the soil's physical and electro-chemical properties are uniform throughout the soil matrix and constant over time, are not as applicable. The changes in the soil properties are predictable within engineering accuracy once the factors that cause the changes are understood. The changes can be integrated into a computational program to refine the approximation of consolidation. In contrast to small strain electro-osmotic consolidation theories where soil properties are assumed unchanged, large strain is taken into consideration for electro-osmotic consolidation to account for changes in soil properties.

For the approximation of large strain consolidation, a suitable point of departure involves a piecewise-linear approximation that is based on Eulerian co-ordinates. Compared with theories[8-10] based on Lagrangian co-ordinates developed to approximate large strain consolidation, the advantages of developing Eulerian co-ordinate-based models include greater versatility regarding initial conditions, boundary conditions and soil heterogeneity[11]. In the piecewise-linear approach, finite elements are integrated over the material's co-ordinate space, whereas in finite differencing, the elements are integrated over time. After each time step, all variables pertaining to the problem geometry, material properties, fluid flow and effective stress are updated with respect to a fixed Eulerian co-ordinate system[12, 13]. The time increment of each step must be sufficiently small so that all variables can be approximated as constants for each iteration. This constraint is a limitation of the piecewise-linear method. However, past studies[11, 14-16] have shown that the piecewise-linear method compares favorably to other large strain formulations and is able to yield validated results with a numerical simulation.

This paper presents a piecewise linear numerical model, called Electro-osmotic Consolidation 1 (EC1), to describe one-dimensional electro-osmotic consolidation. This model is developed with the aid of model CS2[15]. CS2 is a model to approximate vertical consolidation settlement of compressible soil layer. Similar to CS2, EC1 is able to account for a large strain, the soil self-weight, the relative velocity of the fluid and solid phases, and the nonlinear variation of the soil properties (compressibility, hydraulic and electrical conductivity) associated with electro-osmotic consolidation. The constitutive relationships for the soil properties are specified using discrete data points extracted from mathematical approximations or derivative functions of soil properties. The performance of EC1 is verified by comparing its numerical solutions to exact analytical solutions and experimental test results. Example problems involving large-strain settlement and the non-linear constitutive

relationships are illustrated to show the progress of electro-osmotic consolidation. The study presented in this paper continues and complements the content published in one of the authors' recent papers[17], particularly with respect to the experimental setups, the validation of the model and the numerical output results for the example problems.

2. MODEL DESCRIPTION

2.1 Geometry

The initial geometry of a compressible mass prior to the application of a voltage gradient (time $t<0$) is shown in Figure **1**(a). A saturated homogeneous soil mass of initial height H_0, fixed length L and unit width is treated as an idealized two-phase material in which the solid particles and the pore fluid are incompressible. Only vertical compression takes place. Mass continuity is assumed throughout the consolidation process. Electrodes are placed vertically in rows at the two ends, the cathode (–) or the anode (+), of the soil mass. A voltage gradient is generated by applying a voltage across the cathode and anode rows. The length and spacing of the electrodes are configured appropriately so that the electrical field can be approximated as one-dimensional, i.e., along the horizontal dimension across the electrode rows and inducing pore fluid flow in the horizontal direction[18]. Following past investigations[1, 5, 18, 35], the geometry involving horizontal flow is chosen such that fluid moving horizontally is taken to be the usual and efficient consolidation method in practice[19], although electro-osmosis induced vertical flows can be used by using oedometer or triaxial cell-based setups[2, 6, 10, 20, 21].

A vertical Eulerian co-ordinate, z, is defined as positive upward (against gravity) from a fixed datum plane coincident with the bottom of the soil mass. The element co-ordinate j is directed from its origin at the cathode toward its destination at the anode. The soil mass is laterally sliced into R_j elements, each having constant thickness $l_0=L/R_j$, a central node

located at initial elevation z_j^0 and two upper corners located at initial elevations $z_{c,j}^0$ and $z_{c,j-1}^0$. The distribution of the initial void ratio, $e_{0,j}$, within the element j is assumed to be in equilibrium with the effective overburden stress and the self-weight of the soil. The boundaries of the mass can be specified as drained or impermeable. The drainage boundaries are hydraulically accessible to a groundwater table. At t=0, an electrical potential difference, V_m, is applied through the mass. At some later time t (Figure 1(b)), the upper corner heights of the element j are $z_{c,j}^t$ and $z_{c,j-1}^t$. The nodes settle down and remain at the center of their respective elements throughout the consolidation process, and they are updated at each time step.

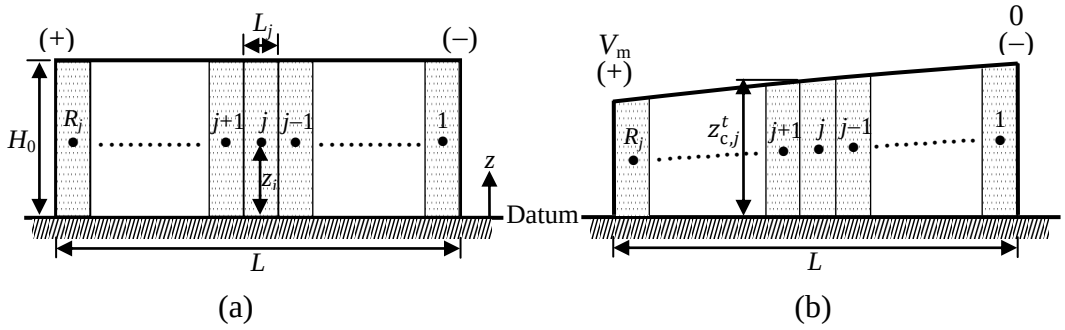

Figure 1: Geometry for EC1: (a) initial configuration (t<0) and (b) configuration after the application of the voltage gradient (t≥0)[17].

2.2 Constitutive relationships

The constitutive relationships for the compressible soil mass are shown in Figure 2, which is adapted from the study CS2[15]. The compressibility curve (Figure 2(a)) is defined by R_m (≥2) pairs of the corresponding void ratio, $\hat{e}$, and the vertical effective stress, $\hat{\sigma}'$. The constitutive relationship of the permeability coefficients (Figure 2(b)) is defined by R_n (≥2) pairs of the corresponding void ratio, $\bar{e}$, and the coefficient of hydraulic permeability, $\bar{k}_h$, or the electro-osmotic permeability, $\bar{k}_e$. The electro-osmotic permeability, $\bar{k}_e$, is defined in a way similar

to that of the hydraulic permeability to quantify the flow rate in response to the voltage gradient, this definition is subsequently elaborated. It is assumed that both permeability coefficients increase monotonically, though in different mathematical forms, as a result of the increase in the void ratio. The trends of the constitutive relationships of the compressibility and permeability are consistent with mathematical forms found in the literature[9, 10, 22-24] and are subsequently discussed and adapted in the computation program to give numerical results. In Figure 2, the superscripts ^ and ¯ are used to distinguish the input values of the void ratio, vertical effectiveness and permeability coefficients that define these curves.

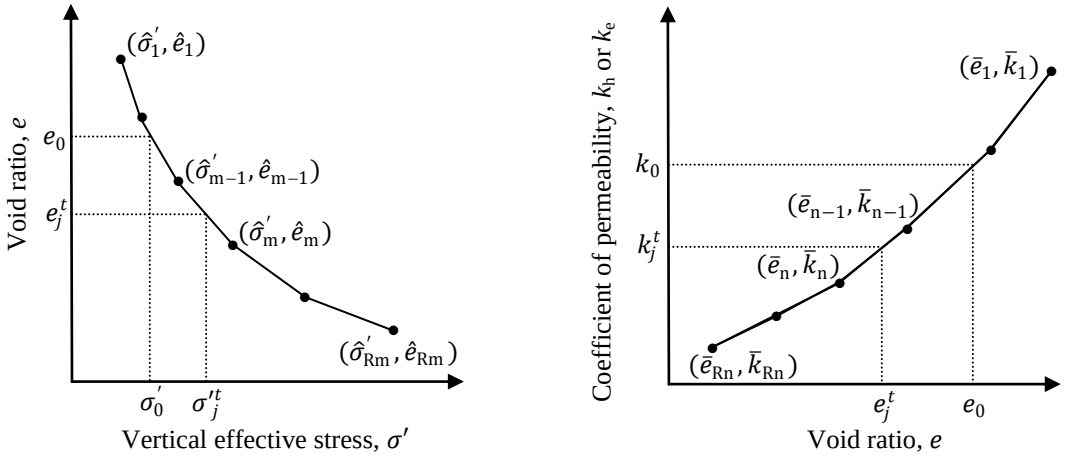

Figure 2: Soil constitutive relationships: (a) compressibility and (b) permeability[17].

There is proportionality between the voltage gradient induced velocity of the fluid flow and the voltage gradient[1, 5]. The proportionality factor is defined as the coefficient of electro-osmotic permeability, k_e. Although the definition of k_e is very similar to that of the coefficient of hydraulic permeability, k_h, which is the proportionality between the hydraulic gradient induced velocity of the flow and the hydraulic gradient, there is a fundamental difference in the two permeability coefficients in that k_e depends mainly on the pore area of soils and is independent of the size of the individual pores, whereas k_h is very strongly

133 influenced by the actual pore size[1]. As a result, there is difference in the mathematical
134 forms for the individual constitutive relationships of the two coefficients.

135 In terms of Figure 2(b), the coefficient of hydraulic or electro-osmotic permeability
136 for element j, k_j^t, is calculated as

$$k_j^t = \bar{k}_{n-1} + \frac{\bar{k}_n - \bar{k}_{n-1}}{\bar{e}_n - \bar{e}_{n-1}}(e_j^t - \bar{e}_{n-1}),\ j=1, 2, \ldots, R_j \tag{1}$$

137 Because the permeability of two contiguous elements will generally not be equal, an
138 equivalent series coefficient of permeability is defined to calculate the inter-element fluid
139 flow. At time t, the equivalent coefficient of permeability, $k_{s,j}^t$, between element j and the
140 prior element (j−1) is

$$k_{s,j}^t = \frac{2k_{j-1}^t k_j^t}{k_{j-1}^t + k_j^t},\ j=2,3, \ldots, R_j \tag{2}$$

141 Regarding Figure 2(b), the relation between the void ratio and the logarithm of the
142 coefficient of the hydraulic permeability of clays, k_h, is also represented in a linear form, as
143 shown in Eq. (3). The linear relation was suggested by Taylor[22] as an empirical form
144 applicable for clays, and it was validated experimentally by Mesri and Olson[3] for the range
145 of void ratio changes encountered in engineering. It has become the most common form of
146 representing the variation of the hydraulic permeability with the void ratio of clays. The
147 experimentally derived constant C_k is the hydraulic permeability index of soil mass.

$$\Delta e / \Delta \log k_h = C_k \tag{3}$$

148 Regarding the constitutive relationship for the electro-osmotic permeability in
149 Figure 2(b), two different mathematical forms were examined for their ability to represent
150 electrical potential driven fluid flow as a function of the void ratio. The first form (Eq. (4)) is
151 based upon the classical Helmholtz and Smoluchowski theory, which was summarized by

Mitchell and Soga[25]. The equation relates the coefficient of electro-osmotic permeability, k_e, to the soil zeta potential, ξ; the dielectric constant of the pore fluid, D; the viscosity of the fluid, η; and the soil porosity, n. Of these values, the porosity is intensively associated with the progress of electro-osmotic consolidation. The second form (Eq. (5)) introduces a threshold coefficient of permeability, k^*, in response to a threshold void ratio, e^*[10, 26]. The threshold values are used to address the effect of the inter-particle interactions on flows, which arises from the thickness variation of electric double layers (i.e., the ionic composition and concentration of the pore fluid). The exponent c in the form offers a second parameter used to correlate k_e with e. Both forms show an approximately linear relationship between k_e and the void ratio e, which was validated in experiments[9, 26].

$$k_e = \frac{\xi D}{\eta} n \tag{4}$$

$$k_e = \begin{cases} k^*; & e > e^* \\ k^* \left(\dfrac{1+e}{1+e^*} \right)^c; & e < e^* \end{cases} \tag{5}$$

To offer a general form of the coefficient of electro-osmotic permeability, Eq. (4) is arranged into Eq. (6), which assumes that the term in the middle of the equation is a constant for a soil in which the ionic composition and concentration of the pore fluid do not change throughout the consolidation of the soil mass. Appling the constant to the initial condition of the soil leads to the term on the right side of Eq. (6). Equation (6) is rearranged into Eq. (7), which means that k_e is predictable given the initial void ratio, e_0, and the initial coefficient of electro-osmotic permeability, k_0. Taking into account the variation of the ionic composition and the concentration of the pore fluid, an experimentally derived exponent, a, is introduced in Eq. (8). This exponent is based on the definition of the exponent c in Eq. (5) and satisfies the pairs of (e, k) obtained in the experimental program.

$$k_{\mathrm{e}}\frac{1+e}{e}=\frac{\xi D}{\eta}=k_{\mathrm{e0}}\frac{1+e_0}{e_0} \tag{6}$$

$$k_{\mathrm{e}}=k_{\mathrm{e0}}\frac{1+e_0}{e_0}\frac{e}{1+e} \tag{7}$$

$$k_{\mathrm{e}}=k_{\mathrm{eo}}\cdot\left(\frac{(1+e_0)\cdot e}{e_0\cdot(1+e)}\right)^{a} \tag{8}$$

172

173 **2.3 Total stress, effective stress, and pore pressure**

174 The vertical total stress at each node in Figure **1** is computed from the applied overburden
175 stress and the self-weight of the compressible mass. In this study, no overburden is applied to
176 avoid vertical flow. Thus, for $t\geq 0$, the total stress at node j, σ_j^t, is

$$\sigma_j^t=z_j^t\times\gamma_j^t,\ j=1,\ 2,\ \ldots,\ R_j \tag{9}$$

177 where γ_j^t is the saturated unit weight of element j,

$$\gamma_j^t=\frac{G_{\mathrm{s}}+e_j^t}{1+e_j^t}\gamma_{\mathrm{w}},\ j=1,\ 2,\ \ldots,\ R_j \tag{10}$$

178 and e_j^t is the corresponding void ratio of element j. G_{s} is the specific gravity of the soil
179 solids, and γ_{w} is the unit weight of water. In EC1, G_{s} and γ_{w} are constant for the
180 compressible mass over the consolidation process, and e_j^t is constant within each element
181 over any given time increment.

182 The vertical effective stress at node j can be computed from e_j^t and the
183 compressibility curve (Figure **2**(a)) as:

$$\sigma'^t_j=\hat{\sigma}'_{m-1}+\frac{\hat{e}_{m-1}-e_j^t}{a_{\mathrm{v},j}^t},\ j=1,\ 2,\ \ldots,\ R_j \tag{11}$$

where the coefficient of compressibility, $a_{\mathrm{v},j}^{t}$, is the slope (absolute value) of the linear segment of the compressibility curve between the points $(\hat{\sigma}'_{m-1},\hat{e}_{m-1})$ and $(\hat{\sigma}'_{m},\hat{e}_{m})$ and equals

$$a_{\mathrm{v},j}^{t} = -\frac{\hat{e}_m - \hat{e}_{m-1}}{\hat{\sigma}'_m - \hat{\sigma}'_{m-1}},\ j=1, 2, \ldots, R_j \tag{12}$$

The form chosen for the compressibility constitutive relationship in Figure 2(a) is commonly represented by a linear relationship, as shown in Eq. (13), between the void ratio, *e*, and the logarithm of the vertical effective stress, σ'. In contrast with the ordinary power law expressions suggested by Feldkamp[9, 10], Eq. (13) offers an explicit relation between *e* and σ' and reduces the number of experimental constants to one. The linear relationship is applicable to normally consolidated soils for all cases and to overconsolidated soils as a first approximation of the compressibility relationship over the appropriate effective stress range for a given problem[24]. Therefore, the compression index, C_c, is assumed to be constant throughout the consolidation process in this study.

$$\Delta e / \Delta \log \sigma' = C_c \tag{13}$$

The pore pressure for node *j*, u_j^t, is the difference between the total and effective stresses, if there are no shear strains between the slices of element.

$$u_j^t = \sigma_j^t - \sigma'^t_j,\ j=1, 2, \ldots, R_j \tag{14}$$

The pore pressure is used to determine the local degree of consolidation in terms of the per cent pore pressure dissipation.

2.4 Electrical resistance and potential

The electrical resistance's dependence on the void ratio is not very clear. Nevertheless, some guidelines are available from the literature to select a reasonable electrical resistivity. Based on the experimental results of Turner[27] and the theoretical work of Fricke[28, 29] on the

suspension of spherically shaped particles, Feldmark[10] suggested a void ratio based formulation to determine the electrical conductivity (the inverse of the electrical resistivity) of soil mass, which assumes that the soil's solid phase has infinite conductance. Based on compressible granular soil, Komine[30] presented, with experimental examination, a parallel model to determine the electrical resistivity of the soil mass, and this model is adapted in this study. Based on Komine's model, at time *t*, the electrical resistivity for element *j*, ρ_j^t, is

$$\rho_j^t = \frac{1}{\frac{1}{\rho_s}\times\frac{1}{1+e_j^t}+\frac{1}{\rho_w}\times\frac{e_j^t}{1+e_j^t}},\ j=1, 2, \ldots, R_j \tag{15}$$

where ρ_s and ρ_w represent, respectively, the electrical resistivity of the solid particle and the pore water. In terms of EC1's geometry (Figure **1**), the electrical resistance of element *j* can be determined as

$$R_j^t = \frac{\rho_j^t \times l_0}{2\times z_j^t},\ j=1, 2, \ldots, R_j \tag{16}$$

An electrical voltage of V_m is applied between the cathode and anode in EC1. If the electrical potential at the cathode is defined as being equal to zero, the electrical potential at the anode is V_m. EC1 doesn't account for, if there are, chemical reactions (such as electrolysis) or physical separations at soil-electrode interfaces or the possible drop of the electrical potential at the interface. Hence, the voltage input value for EC1 is V_m, less the potential drop at the electrodes, which is accommodated in subsequent study of model validation. For the numerical output of this study, it is assumed that there is no drop at the interface and the voltage input value is V_m. At time *t*, the electrical potential at node *j*, V_j^t, is

$$V_j^t = \frac{\frac{R_j^t}{2} + \sum_{i=1}^{j-1} R_i^t}{\sum_{i=1}^{R_j} R_i^t} v_m \,,\ j=1, 2, \ldots, R_j \tag{17}$$

221

222 **2.5 Fluid flow and settlement**

223 There are two opposite fluid flows superimposed in the compressible mass for one-
224 dimensional electro-osmotic consolidation[5, 31], i.e., the flow as a result of the hydraulic
225 gradient and the one in response to the voltage gradient of the unit strength. The hydraulic
226 gradient is generated in response to the differential negative pore pressure, increasing from
227 the cathode toward the anode, thus the differential consolidation along the flow path[5]. The
228 rate of flow is quantified by introducing the coefficient of hydraulic permeability, k_h, and the
229 coefficient of electro-osmotic permeability, k_e. For EC1, the flows are illustrated in Figure **3**.
230 At time *t*, the volume of the fluid flow between two contiguous elements, *j* and (*j*−1),
231 includes two components, i.e., the flow volume induced by the hydraulic gradient, $q_{h,j}$ (Eq.
232 (18)), and the flow volume by the voltage gradient, $q_{e,j}$ (Eq. (19)). The total volume of the
233 fluid flow is the superposition of the two components.

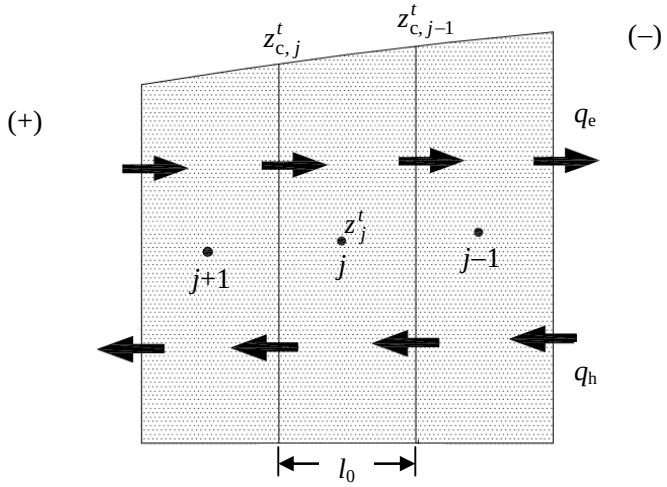

Figure 3: Water flow between individual elements.

$$q_{\mathrm{h},j} = k^t_{\mathrm{hs},j} i^t_{\mathrm{h},j} A^t_j,\ j=1, 2, \ldots, R_j \tag{18}$$

$$q_{\mathrm{e},j} = k^t_{\mathrm{es},j} i^t_{\mathrm{e},j} A^t_j,\ j=1, 2, \ldots, R_j \tag{19}$$

where $k^t_{\mathrm{hs},j}$ and $k^t_{\mathrm{es},j}$ define the equivalent series coefficients of the hydraulic permeability and the electro-osmotic permeability between contiguous elements, j and (j–1), respectively, and are determined in terms of Eq. (2). A^t_j defines the average area of the cross section between the elements. $i^t_{\mathrm{e},j}$ and $i^t_{\mathrm{h},j}$ define the voltage gradient and the hydraulic gradient between two contiguous elements, j and (j–1), respectively, and are

$$i^t_{\mathrm{e},j} = \frac{V^t_j - V^t_{j-1}}{l_0},\ j=1, 2, \ldots, R_j \tag{20}$$

$$i^t_{\mathrm{h},j} = \frac{h^t_{j-1} - h^t_j}{\sqrt{l_0^2 + (z^t_{j-1} - z^t_j)}},\ j=1, 2, \ldots, R_j \tag{21}$$

where h^t_j defines the total head of node j and is

$$h^t_j = z^t_j + \frac{u^t_j}{r_{\mathrm{w}}},\ j=1, 2, \ldots, R_j \tag{22}$$

Following the fluid flow, at time ($t+\Delta t$), the cross-section area of the element j, $A^{t+\Delta t}_j$, relative to its area at time t, A^t_j, is

$$A^{t+\Delta t}_j = A^t_j - (q^t_{\mathrm{e},j} - q^t_{\mathrm{e},j+1} - q^t_{\mathrm{h},j} + q^t_{\mathrm{h},j+1}) \times \Delta t,\ j=1, 2, \ldots, R_j \tag{23}$$

and the void ratio, $e^{t+\Delta t}_j$, is

$$e^{t+\Delta t}_j = \frac{A^{t+\Delta t}_j \times (1+e^0_j)}{A^0_j} - 1,\ j=1, 2, \ldots, R_j \tag{24}$$

At time ($t+\Delta t$), the settlement of element j, $s_j^{t+\Delta t}$, the average settlement of the soil mass, $s_{\text{avg}}^{t+\Delta t}$, and the average consolidation degree for the soil mass, $U_{\text{avg}}^{t+\Delta t}$, are

$$s_j^{t+\Delta t} = H_0 - (z_{\text{c},j}^{t+\Delta t} + z_{\text{c},(j-1)}^{t+\Delta t})/2,\ j=1, 2, \ldots, R_j \tag{25}$$

$$s_{\text{avg}}^{t+\Delta t} = \frac{\sum_{j=1}^{Rj}(A_j^0 - A_j^{t+\Delta t})}{L} \tag{26}$$

$$U_{\text{avg}}^{t+\Delta t} = \frac{s_{\text{avg}}^{t+\Delta t}}{s_{\text{avg}}} \tag{27}$$

where s_{avg} is the average final settlement of the soil mass when one component of the flow completely offsets the other and there is no more settlement. In EC1, the offset is reached when the settlement difference of two contiguous time steps is less than a sufficiently small number.

2.6 Boundary drainage conditions

The boundary drainage conditions are configured in terms of the choices of the access to water at the electrodes and the upper/lower boundary surfaces of the geometry (Figure **1**). The boundary is open if the electrode or surface is free to access water. It is closed if no water is allowed to flow inward or outward. In EC1, the flow of fluid is directed in the horizontal dimension, and no flow occurs across the upper and lower boundaries. At the electrodes, the boundaries vary depending on whether free water is maintained outside the electrodes, which leads to imposing two variables, the total head for the water adjacent to the cathode, h_{w1}, and that for the water adjacent to the anode, h_{w2}. The variables are set zero when the electrodes are closed without free access to water, or a number is entered to reflect the hydraulic conditions outside the electrodes.

Table 1 shows the hydraulic and electrical boundary drainage conditions at the electrodes for EC1. At the cathode, if the boundary of the soil mass is sealed without access to water supply, the requirement of zero flux for element 1 must be imposed, leading to $i^t_{e,1} = 0$ and $i^t_{h,1} = 0$. On the other hand, if the boundary at the cathode is perfectly drained, the voltage gradient and hydraulic gradient for element 1 are $i^t_{e,1} = 2V_1/l_0$ and $i^t_{h,1} = 2(h_{w1} - h^t_1)/l_0$, respectively. Similar boundary drainage conditions are defined for the gradients through element R_j at the anode. In practice, the boundary drainage is often defined the same way, i.e., open cathodes and closed anodes. Scenarios of such boundary drainage conditions are supposed to facilitate the draining of fluid out of the soil mass. In these scenarios, the boundaries at the cathodes are open to discharge the gathered volume of water through vertical drains (referred to as sandwicks) by vacuum pumping[18, 32], and the boundaries at the anodes are closed to block the possible in-flow of water from adjacent soils.

Table 1: EC1 boundary drainage conditions.

	Closed	Open
At cathodes	$i^t_{e,1} = 0$ and $i^t_{h,1} = 0$	$i^t_{e,1} = 2V_1/l_0$ and $i^t_{h,1} = 2(h_{w1} - h^t_1)/l_0$
At anodes	$i^t_{e,Rj} = 0$ and $i^t_{h,Rj} = 0$	$i^t_{e,Rj} = 2(V_m - V_{Rj})/l_0$ and $i^t_{h,Rj} = 2(h^t_{Rj} - h_{w2})/l_0$

2.7 Time increment

EC1 adapts the criteria used in CS2[15] to determine the time increment Δt. Because EC1 is developed in a form analogous to CS2, including the definition of the fixed co-ordinate, element slicing, flow mass continuity, constitutive relations and iterative algorithm, the criteria of the defining time increment in CS2 are inherently valid for EC1. For simplicity, the time increment is calculated as the minimum of three criteria:

$$\Delta t_j = \min\left\{ \frac{\alpha a_{\mathrm{v},j}^t l_0^2}{k_j^t (1+e_j^t)},\ \left| \frac{0.01 s_{0,j}(e_{0,j}-e_{\mathrm{f},j})}{(1+e_{0,j})(q_{j-1}^t - q_j^t)} \right|,\ \left| \frac{0.01 s_{0,j}(e_{0,n}-e_{\mathrm{f},n})}{(1+e_{0,n})(q_n^t - q_b^t)} \right| \right\},\ j=1, 2, \ldots, R_j \qquad (28)$$

where α is a constant ≤0.5. The time increment is most accurate for $\alpha \cong 0.4$.

3. EC1 COMPUTER PROGRAM

Figure 4 shows a flow chart illustrating the basic algorithm for the program. The input data are the number of elements (R_j), the applied voltage (V_m), the specific gravity of the solids (G_s), the initial dimension of the soil mass (H_0, L), the data points for the constitutive relationships, the boundary drainage conditions and the termination criteria for the program. The number of elements is dependent on the accuracy and computation time. After EC1 reads the initial input data of element j (l_0 z_j $z_{\mathrm{c},j}$ $e_{0,j}$) and the voltage (V_m), the calculation loop begins at the time step Δt. Following each time step, the pore pressure, effective stress, void ratio, electrical resistivity, and coefficients of the hydraulic and electro-osmotic permeability are then calculated for each element based on the specified constitutive relationships. The volume of the flow, the new heights of each element, the average settlement of the soil mass, and the local and average degrees of consolidation are then calculated. Program execution terminates when $t \geq t_\mathrm{f}$ or $\Delta s_{\mathrm{avg}} \leq m$, where t_f and m are, respectively, the user-specified elapsed time and a sufficient small value of the settlement difference. When m is reached, the two opposite flows in response to the hydraulic gradient and the electro-osmotic gradient are in equilibrium. The average settlement is then the final settlement s, and it is used to calculate the average consolidation degree, U_{avg}^t.

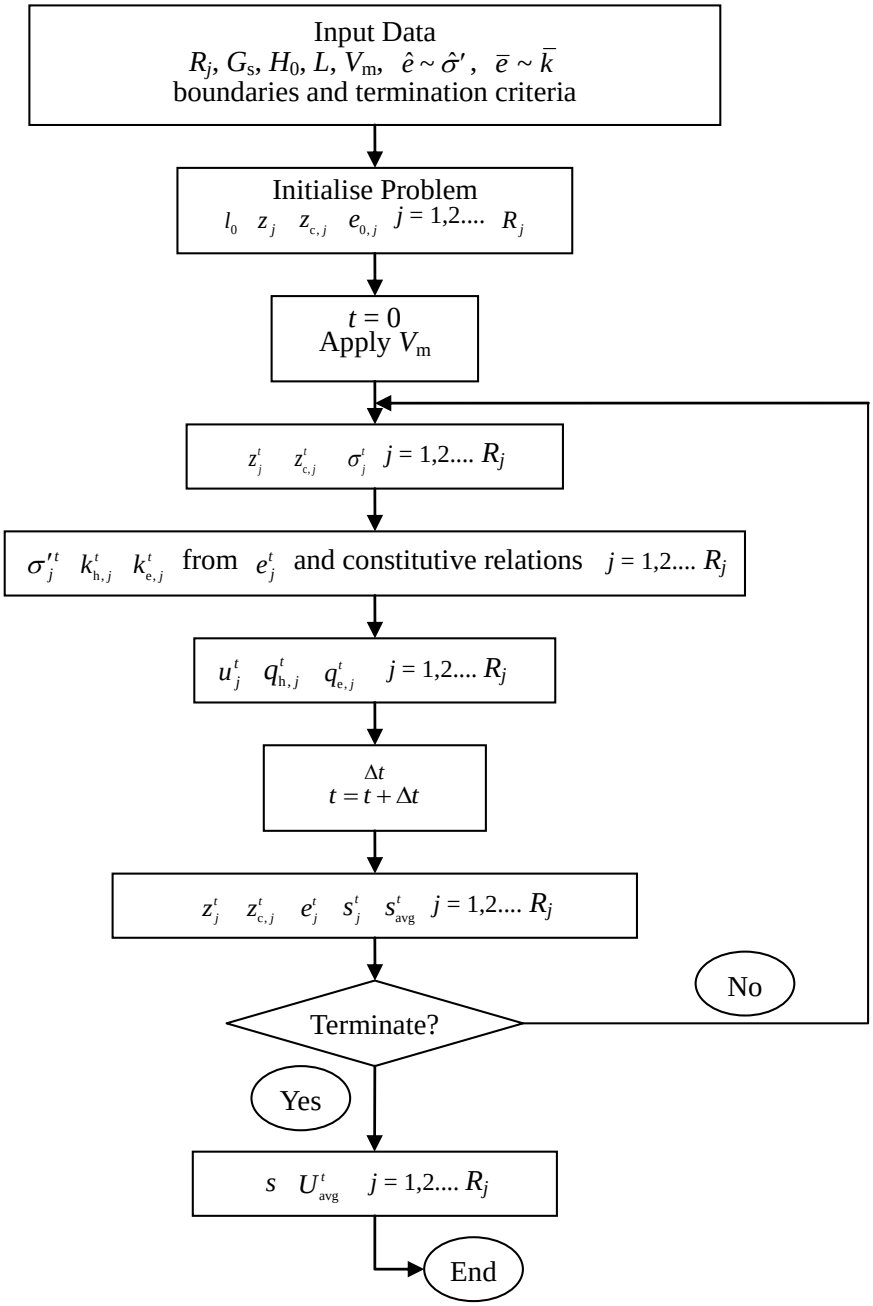

Figure 4: Flow chart for EC1.

4. MODEL VERIFICATION

The performance of EC1 is verified against the analytical exact solutions given by Esrig[5] with respect to uniform and saturated soil subjected to one-dimensional small-strain electro-osmotic consolidation. An experimental program is subsequently presented to further validate the accuracy of the model's approximation for when large-strain settlement takes

place and the soil's physical and electro-chemical properties change throughout the electro-osmotic consolidation of the soil.

4.1 Verification against exact solutions

The geometry of Esrig's one-dimensional solutions is identical to the one shown in Figure **1,** which involves horizontal flow between the cathode and anode rows. EC1 is configured to take into account those exact solutions, which makes it possible to verify EC1 against the solutions. The exact solutions assume a small strain and take the physical and electro-chemical properties of the soil mass to be constant. The input values of the properties are shown in Table **2**. The coefficient of compressibility, a_v, is 0.005 kPa^{-1} (e.g., for plastic clay under a common range of pressures), a constant resulting in a straight line of the compression curve of Figure **2**(a) (linear compressibility). Further input values are 2×10^{-9} m/s for the coefficient of hydraulic permeability, k_h, and 5×10^{-9} $m^2/s\cdot V$ for the coefficient of electro-osmotic permeability, k_e. Both coefficients are constant over time. The other input values are 1 for the void ratio, e_0; 1×10^{-5} V for the electrical potential difference, V_m, between the anode and the cathode rows; and 1 for the specific gravity of the solid particle, G_s (no self-weight). The electrical potential difference is deliberately set at a sufficiently low value to validate the assumption of small-strain deformation.

Table **2**: Model validation: input data for the soil properties and model geometry.

Variable	Value
Coefficient of compressibility, a_v (kPa^{-1})	0.005
Coefficient of hydraulic permeability, k_h (m/s)	2×10^{-9}
Coefficient of electro-osmotic permeability (initial), k_e ($m^2/s\cdot V$)	5×10^{-9}
Initial void ratio, e_0	1

Applied voltage, V_m (V)	1×10^{-5}
Specific gravity, G_s	1
Unit weight of water, γ_w (kN/m^3)	9.8
Length of soil mass, L (m)	1
Height of soil mass, H_0 (m)	1
Number of elements for soil mass, R_j	20, 50, 100 or 200

Referring to the geometry in Figure 1, the soil mass is L=1 m long, H_0=1 m deep and 1 m wide. Between the electrodes, the 1 m long soil mass is sliced into R_j = 20, 50, 100, and 200 elements to consider the effect of the element slicing number on the computational accuracy of EC1. As a result, the thickness of an element ranges from 5 to 50 mm, which is less likely to invalidate the coefficients of the inter-element flow permeability (Eqs. (1) and (2)). It is important to note that the variation of the element thickness does not affect the compressibility and permeability of each element.

Esrig[5] provided an exact solution to the average consolidation degree, U_{avg}, under the drainage boundaries of a sealed anode, an open free draining cathode and h_{w1}= 0 for the total head of water outside the cathode, which, as previously mentioned, is the most common drainage boundary in practice. As a first approximation, the U_{avg} obtained under such boundaries was used for the purpose of verification. In terms of the geometry of Figure 1, the final settlement, s_x, of the soil at any position x (originating from the cathode toward the anode) is

$$s_x = \frac{a_v \left| u_f(x) \right|}{1+e_0} H_0 \tag{29}$$

where the final pore pressure $u_f(x)$ at position x was derived by Esrig[5] as

$$u_{\mathrm{f}}(x) = -\frac{k_{\mathrm{e}}\gamma_{\mathrm{w}}V_{\mathrm{m}}}{k_{\mathrm{h}}}\left(\frac{x}{L}\right) \tag{30}$$

Averaging s_x over the length, L, of the soil mass gives the final average settlement of the soil.

$$s_{\mathrm{avg}} = \frac{a_{\mathrm{v}}k_{\mathrm{e}}\gamma_{\mathrm{w}}V_{\mathrm{m}}}{2k_{\mathrm{h}}(1+e_0)}H_0 \tag{31}$$

Table 1 shows the output results of U_{avg} as a function of the time factor, T_{v}. The second column gives the results from exact analytical solutions, and the remaining columns show the numerical results obtained by running EC1 with 20, 50, 100 and 200 elements. Using a 2.2 GHz desktop unit, the required computation time for these solutions was 0.5, 1, 10 and 67 s for R_j=20, 50, 100 and 200, respectively. Each column of the numerical results is in satisfactory agreement with the analytical results, and the accuracy improves as the number of elements increase. When the soil mass is refined into 100 elements (an element is 10 mm thick) or higher, the numerical results are optimized and are an ideal match with the results of Esrig's solutions. That is, the choice for R_{j} depends on the desired solution accuracy and the acceptable computation time. A value of R_{j} between 50 and 100 is able to give plausible results, which coincides with the findings in a previous study[15]. Through the comparison of results, it is verified that EC1 represents the correct formulation for the approximation of the one-dimensional electro-osmotic consolidation of small strain.

Table 1. Comparison of the average consolidation degree.

T_{v}	U_{avg} (%)				
	Esrig's solution	EC1			
		R_j=20	R_j=50	R_j=100	R_j=200
0.04	7.999	8.079	8.012	8.002	8.000
0.08	15.923	16.001	15.936	15.926	15.924
0.12	23.510	23.583	23.522	23.513	23.511
0.20	37.039	37.100	37.048	37.041	37.039
0.25	44.321	44.375	44.328	44.323	44.322
0.35	56.486	56.529	56.492	56.487	56.486
0.45	65.999	66.032	66.003	66.001	65.999
0.6	76.517	76.539	76.521	76.518	76.517
0.8	85.664	85.677	85.666	85.664	85.664

1.2	94.657	94.662	94.658	94.657	94.657

Figure 5 shows the distribution of the pore pressure over time when the number of elements, R_j, is 100. Based on Esrig's solutions, the vertical axis takes the normalized dimensionless distance of x over the length of the soil mass L, while the horizontal axis represents the pore pressure normalized against the maximum pore pressure. In the figure, the continuous lines indicate the analytical results obtained from the exact solutions, and the discrete squares represent the numerical results of EC1. The numerical results of the pore pressure fall on the lines and suggest a close approximation against analytical results. The results show that the pore pressure at the cathode is zero throughout consolidation because of the open boundary of the cathode. The pore pressure at the anode increases over time because the drainage boundaries are closed. As a result, the distribution of the pore pressure over the soil mass has a triangular shape at infinite time.

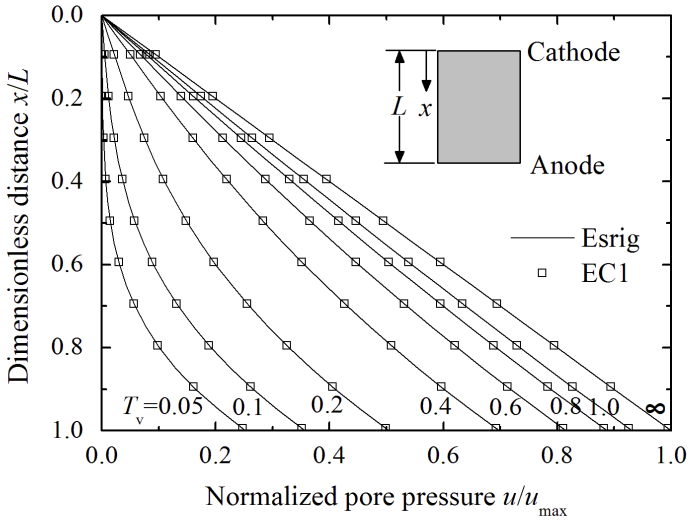

Figure 5: Comparison of the pore pressures over time and distance.

4.2 Verification through experimental tests

4.2.1 Materials

The materials used in the experimental tests were fine-grained kaolin, which is a chemically stable mineral material and widely deployed as a model clayey soil for the approximation of electrokinetic tests[33, 34]. The physical properties of the kaolin are shown in Table 3. The plastic and liquid limits were obtained by using the fall cone method. The water content of the kaolin used for electro-osmotic consolidation was 50.7%, which turned the soil into a liquid. One of the purposes of setting a high water content for kaolin is to simulate the water content of soils in the field (e.g. hydrofills). The other purpose is to allow sufficient consolidation and thus large strain deformation which is of the aim of this study. The soil was saturated by vibrating and mixing the soil into a viscous paste before backfilling the soil into experimental setups. The initial void ratio was calculated through the known properties of the specific gravity, water content and saturation degree. A part of the prepared kaolin was subjected to an odometer test, which gave a coefficient of compressibility, a_v, of 3.66×10^{-4} kPa^{-1}, and compression index, C_c, of 0.19. The value of a_v was determined as the gradient of the approximation line for observations between 0 and 800 kPa in the *e-p* curve of the soil, which suggests an average value for the coefficient of compressibility. The odometer test was conducted using a Rowe-type consolidation cell equipped with pressure/volume controllers. The odometer cell was also used to obtain the results for the initial coefficient of hydraulic permeability, k_{h0} equal to 1.08×10^{-9} m/s, and the hydraulic permeability index, C_k equal to 0.99.

Table 3: Physical and electrical properties of kaolin.

Property	Value
Plastic limit, w_P (%)	22.2
Liquid limit, w_L (%)	43.7
Specific gravity, G_s	2.62

Water content, w (%)	50.7
Initial void ratio, e_0	1.31
Coefficient of compressibility, a_v (kPa^{-1})	3.66×10^{-4}
Compression index, C_c	0.19
Coefficient of hydraulic permeability (initial), k_{h0} (m/s)	1.08×10^{-9}
Hydraulic permeability index, C_k (Eq. (3))	0.99
Coefficient of electro-osmotic permeability (initial), k_{e0} (m^2/s·V)	4.03×10^{-9}
Electrical resistivity of the pore fluid, ρ_w (Ω·m)	4.5
Electrical resistivity of the solid particle of kaolin, ρ_s (Ω·m)	608

A permeameter was developed to measure the coefficient of electro-osmotic permeability, k_{e0}. The schematic of the permeameter is shown in Figure 6. The permeameter is designed to allow hydraulic and electro-osmotic flows simultaneously or separately through the soil sample of kaolin. The hydraulic flow is provided by two standpipes, *a* and *b*, which are connected to the outlet at the top of the permeameter and to the inlet at the bottom, respectively. The electro-osmotic flow is driven by the voltage gradient, i_e, between two circular electrode discs that are placed above and below the soil sample. The electrode discs are made of a piece of steel mesh sheet for the cathode and a perforated graphite pad for the anodes. The soil sample, 4 cm high, is exposed purely to the hydraulic gradient, i_h, if no voltage gradient is applied, which satisfies the falling head method and provides the measurement of the coefficient of permeability of the soil, k_h. When exposing the same soil to the voltage gradient, i_e, only, the water heads in the standpipes rise to different levels and reach equilibrium in response to the electro-osmotic flow. The equilibrium satisfies Eq. (32)[5, 25], which calculates the coefficient of electro-osmotic permeability, k_e. In contrast to pure osmotic-flow methods[1], the advantage of using this method identifies the flow rate relevant to the electro-osmotic flow and then calculates k_e

401 rather than calculating k_e in terms of the combination of both the hydraulic and electro-
402 osmotic flows.

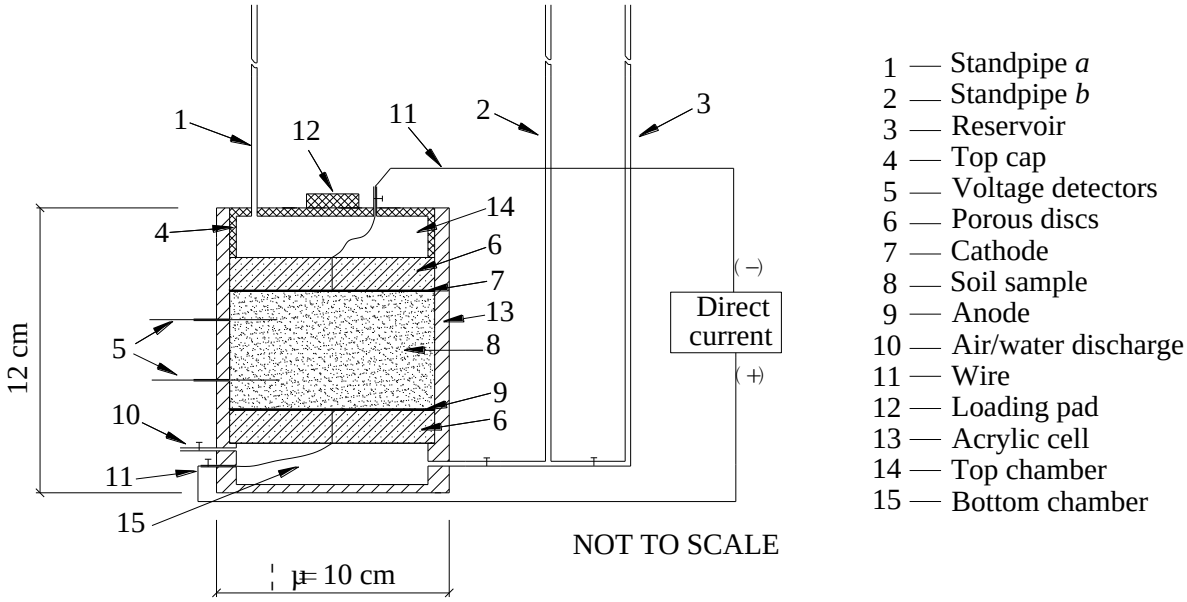

Figure 6: Schematic of the hydraulic and electro-osmotic permeameter.

$$k_h i_h = k_e i_e \tag{32}$$

403 Figure 7 shows the results of the electro-osmotic permeability, k_e, in response to the
404 void ratio, e, of the five soil samples that were exposed to a voltage gradient of i_e=10 V/m.
405 The results of k_e and e were used to calibrate the exponent a in Eq. (8), which was 3.5 for the
406 soil of kaolin. Along with the increase of the void ratio, the electro-osmotic permeability of
407 the soil increases, which means that the higher the porosity of the soil is, the more the flow
408 rate is increased by the voltage gradient, given that the other material properties remain
409 unchanged. The relation does not show the effect of the pore size on the permeability, which
410 will be investigated in a future study. For a void ratio ranging from 0.79 to 2.21, the value of
411 k_e varies from 2.1×10^{-9} to 7.3×10^{-9} $m^2/s\cdot V$, which is comparable to the order of magnitude of
412 the test results for clayey soils reported in previous studies[1, 2, 20]. For the kaolin sample

subjected to electro-osmosis tests, the initial coefficient of electro-osmotic permeability, k_{e0}, was 4.03×10^{-9} $m^2/s\cdot V$ (Table 3) when the initial void ratio, e_0, of the soil was 1.31.

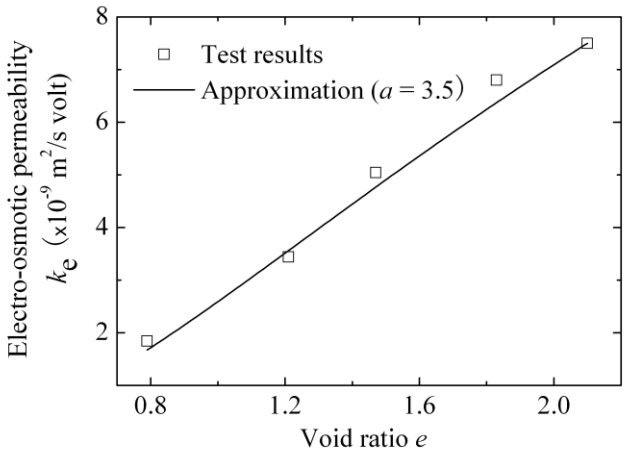

Figure 7: Relation between the electro-osmotic permeability and the void ratio.

The last two properties in Table 3 are the electrical resistivity of the pore fluid and the solid particle of kaolin, which were determined using an M.C. Miller soil box. The schematic of the box and its peripheral circuit are shown in Figure 8. The dimensions of the box are 40 mm (W) × 40 mm (D) × 100 mm (L). At the ends of the box, the electrodes of aluminum pads are installed to apply a voltage gradient through the soil sample of kaolin. During the tests, two copper needles were inserted vertically over the center part of the soil, into the soil at a distance of l=46 mm and to the depth of approximately 20 mm. In terms of Ohm's Law, the readings of the voltmeter and current meter were combined to calculate the electrical resistivity of the kaolin-water mixture ρ_{sw}. A series of seven kaolin samples were prepared at different water contents w and void ratios e, which were used to provide the relation between ρ_{sw} and w or e (Figure 9). The relation was then approximated against Eq. (15), which was implemented by using the Fitting Function Organizer tool in OriginPro 8.0, a data analysis and graphing software package. The approximation resulted in the estimates of two dummy

variables in Eq. (15), i.e., the electrical resistivities of the pore water, ρ_w = 4.5 Ω·m, and the solid particle, ρ_s =608 Ω·m. The error of the approximation was less than 5% when the approximated results were compared against the test results, which indicates the validity of the approximation.

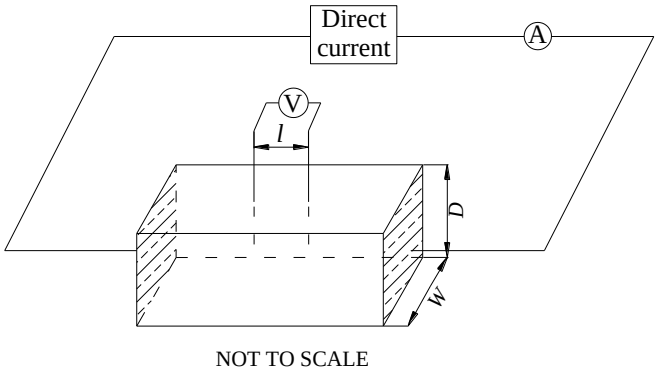

Figure 8: Schematic of the Miller soil box and the peripheral circuit.

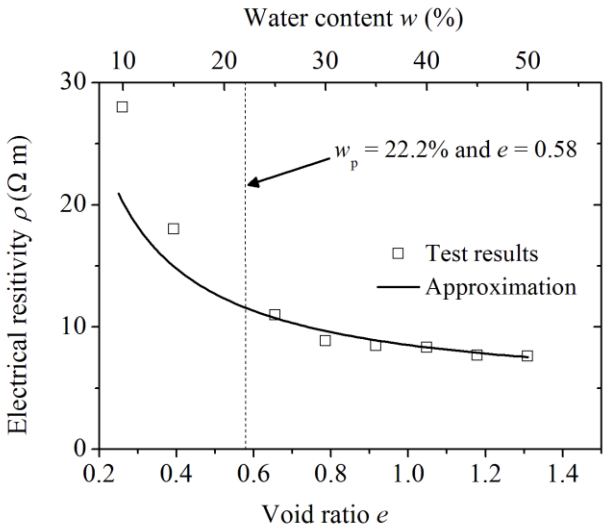

Figure 9: Resistivity of the kaolin-water mixture against the void ratio and water content.

The above approximation reflects the ion concentration of the pore fluid and the diffusion double layer of the solid particle of the soil. It is acknowledged that the resistivity of any material is dependent on the amount of free ions and the valence values of the ions.

For soils, the ion concentration of the pore fluid and the exchangeable ions of the solid particles are neither accessible to measure nor constant during the electro-osmotic consolidation process. Thus, measuring the exact resistivities of the pore fluid or the solid particle of the soils is not feasible. The above approximation adapts the resistivity approximation used by Komine[30] and validates itself to a satisfactory extent.

The results in Figure 9 indicate that the electrical resistivity of the kaolin-water mixture is associated with the water content (or void ratio) of the mixture. Overall, the resistivity decreases along with the increase of the water content, which is due to the low resistivity of water relative to that of the soil solid particle. Furthermore, when the water content is less than the plastic limit of the kaolin (on the left side of the plastic limit), the resistivity decreases significantly with an increase in the water content. On the right side of the plastic limit, however, the resistivity decreases marginally with an increase in the water content. The majority of the water volume in a soil matrix is in the form of absorbed water affixed by the bond force onto the surface of solid particles when the water content is less than the plastic limit of the soil. Otherwise, the volume is in the form of free water. That is, the adsorbed water where ions concentrate tends to enhance the transmission of electrical current more efficiently than free water.

4.2.2 Experimental setup for electro-osmotic consolidation

Figure 10 shows the schematic of the experimental setup used to conduct one-dimensional electro-osmotic consolidation. The setup consists of a consolidation box and its peripheral circuit. The dimensions of the box are 25 cm (W) × 20 cm (D) × 36 cm (L). The box is divided into two compartments of 33 cm (L_1) and 2 cm (L_2). The compartment 33 cm long is reserved for the backfill of kaolin, while the other is used for water collection or drainage. Between the two compartments, a 1 cm thick composite pad is installed as the

cathode of the apparatus, which sequentially consists of a layer of geofabric (as filter), a piece of steel mesh sheet (as electrode) and a perforated polycarbonate pad to retain the dimensions of the kaolin. The position of the composite pad is flexible to allow for the change of the length of the soil compartment. The other end of the soil compartment is used for the installation of the anode, which is a row of graphite rods. Graphite rods are relatively inert and often used as the materials for anodes in order to mitigate oxidation corrosion to the anodes.

The sample soil of kaolin in Table 3 was placed and tamped in layers into the box. The final height of the soil was 17 cm. The electrodes were subjected to a direct current of a voltage of 45 V during the electro-osmotic consolidation process. The electrical potential was measured at separate positions, i.e., 7.5, 14.5, 18.5, 22.5 and 29.5 cm away from the cathode. The effective voltage was assessed by eliminating the potential drop at the electrodes-soil interface. Specifically, electrical potentials were measured at 5 mm away from the anode and the cathode to identify the potential drops at the electrodes. The volume of discharged fluid was collected at the cathode for up to 72 hours and measured every one hour for the first day, every two hours for the second day and every four hours for the third day, except during the night.

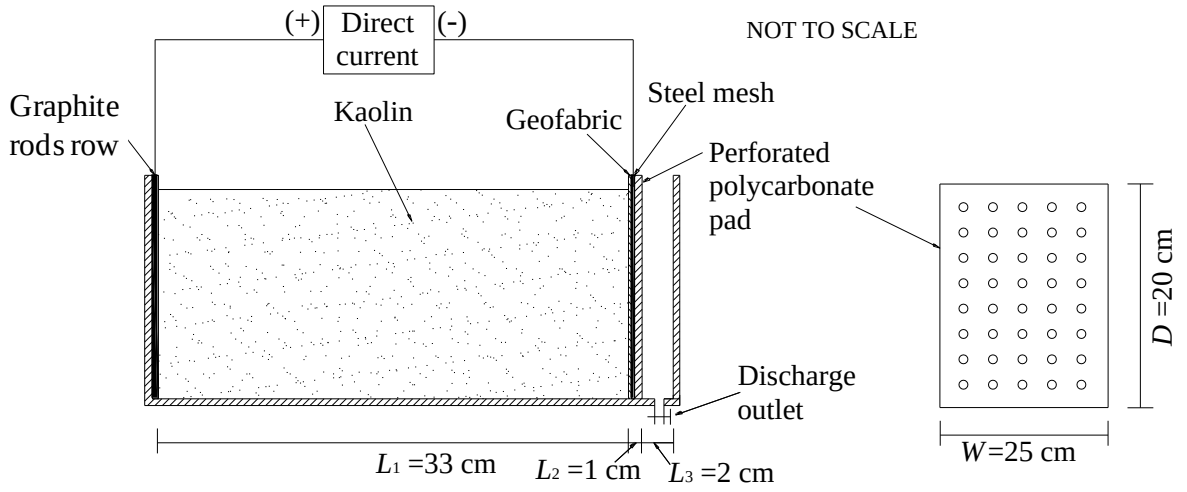

Figure **10**: Schematic of the electro-osmotic consolidation box and the peripheral circuit.

4.2.3 Electrical potential

Figure **11** shows the observed and computed distributions of the effective electrical potential at 0, 12, 24, 48 and 72 hours. The effective voltage is the applied voltage and is less than the potential loss or drop along the electrodes-soil interface. The main drop of the potential occurs to the soils in the proximity of the anodes, where electro-chemical corrosion and physical separation take place and deteriorate the electrical conductivity of the soil mass. The potential drop was reported in the proximity of the cathode in a recent study[20]. The difference in the potential drop position may be ascribed to the different direction of the flow involved in the two studies. That study involves vertical flow, which was simulated in the cell of a modified triaxial compression apparatus, and the anode was at the bottom of the cylindrical sample and the cathode at the top so that the soils remain in contact with the anode.

The effective voltage decreases nonlinearly over time, diminishing from 40 V at start to 14 V after 72 hours, which leads to a potential efficiency factor (the ratio between effective voltage and applied voltage) of 14/40=35%. The efficiency factor is much less than those (56.9% to 66.7%) reported by Jeyakanthan et al.[20] and is comparable to the factors (27.5% to 67.6%) by Mohamedelhassan and Shang[35]. Jeyakanthan et al.[20] installed upright samples and applied electrical field in vertical dimension so as to avoid the electrical potential drops at anodes, which is one of the major causes that lead to higher efficiency factor. Mohamedelhassan and Shang[35] used a tube for making soil samples and applied electrical field in horizontal dimension which was adopted in this study. Consequently, comparable values of efficiency factors were obtained.

The values of the effective voltage are inputted into EC1 to calculate the electrical potential over time. The values of the potential are in close agreement for each plot in Figure **11**. The electrical potential varies nonlinearly over the measurement positions and throughout the elapsed time. Starting with a linear distribution (t =0), the distribution of the potential develops into a series of concave curves corresponding to various elapsed times.

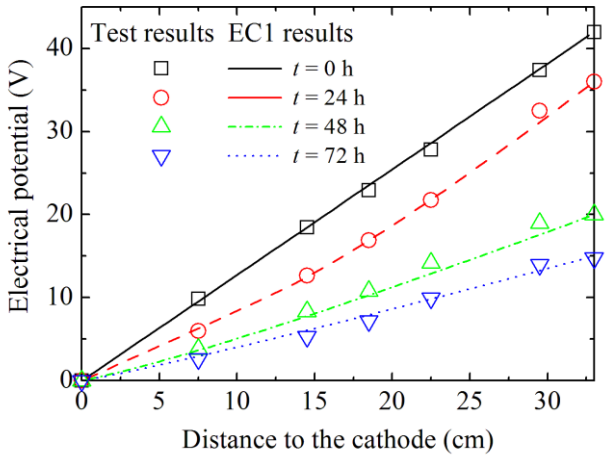

Figure **11**: Validation: the electrical potential vs. the distance to the cathode.

4.2.4 Rate of flow

The flow rate of water was examined to verify the accuracy of EC1 experimentally. The rate is defined as the volume of water discharge against the elapsed time, and this definition was also adapted in a previous study[1]. In addition to experimental observations, Esrig's exact solution of the rate of flow was also used to verify the accuracy of EC1. Given Esrig's exact solutions to the average consolidation degree, U_{avg}^{t}, at time t, the volume of flow, q^{t}, at time t is

$$q^{t} = q_{\text{final}} \times U_{\text{avg}}^{t} \tag{33}$$

where q_{final} is the final volume of the flow and is

$$q_{\text{final}} = L \times W \times s_{\text{avg}} \tag{34}$$

where L and W are, respectively, the length and width of the soil mass, and s_{avg} is the final average settlement of the soil and refers to Eq. (31).

The values of the effective voltage were used to calculate the rate of flow, which is shown in the upper part of Figure **12**. It is seen that the effective voltage drops over time. Per measurements (Figure **11**), the drop occurred to the soils in the proximity of the anodes. There are two main reasons related to the potential drop at the anode-soil interface. The anodes are places where oxidation reactions occur heavily. More or less, the materials of the anodes are corroded and end up with a film of precipitation of metal oxides which pose higher resistance than the native materials. As a result, a portion of electrical potential is consumed at the interface. The other reason is associated with the physical gaps and cracks occurred respectively to the anode-soil interface and the soils around the anodes. The gaps and cracks are raised due to the escape of water and climb-up of negative pore pressures in the proximity of the anodes. Similar to the consequence of the film of oxides, the gaps and cracks raise the electrical resistivity of soil mass and consume extra electrical potential.

The lower part of Figure **12** shows the observations of the flow rate, its exact solutions, and the approximation results provided by EC1 when the soil mass was sliced into 50 elements (R_i =50). The approximation results are in closer agreement with the observations than the exact solutions, which means EC1 outperforms the exact solutions when large-strain settlement occurs. The exact solutions underestimate the flow rate after 8 hours. The underestimation is associated with the determination of the coefficient of compressibility, a_v, which is one of the input data for the exact solutions (Eqs. 29 and 31). The coefficient a_v, the gradient of the secant line in a compressibility (*e*-*p*) curve, is a variable and the value of a_v is dependent on the level of stresses of the secant line. The higher the stress, the lower the value of a_v, and the less compressibility of the soil. The value of a_v (in

Table 3) for Esrig's solutions was determined as the gradient of the approximation line for observations between 0 and 800 kPa. The approximated value was less than the one at low level stress and greater than the one at high level stress. As a result, the input of the approximated value of a_v progressively underestimated the discharge of fluid. Further discussions about the effect of value of a_v on consolidation estimation can be found in previous publications[36-37].

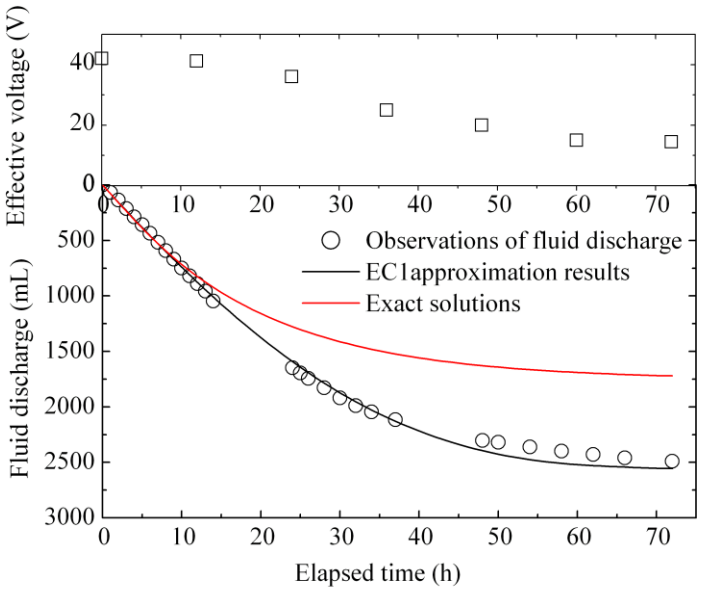

Figure 12: Validation: the volume of flow vs. the elapsed time.

5. NUMERICAL RESULTS

Example problems are illustrated to analyze the electro-osmotic consolidation of a compressible soil mass that involves large-strain deformation. Table 4 gives the input data for example problems. The problems involve the geometry of soil of 1 m long, 1 m high and unit width. The problems focus on the effect of the voltage gradient on the progress of electro-osmotic consolidation. The range of the voltage gradient i_e varies from 10 V/m to 50 V/m, which is consistent with the gradient of 30 V/m or so usually used in practice[38]. The

compressibility and hydraulic conductivity constitutive relationships are included to study the effect of the nonlinear variation of the physical properties on consolidation. The constitutive relationships are shown in Eq. (13) for the compressibility and Eq. (3) for the hydraulic conductivity. The constants on the right side of both constitutive relationships equal 1 to allow for the large-strain deformation of compressible clay soils. The constitutive relationship of the electro-osmotic permeability is also taken into account to analyze the effect of the permeability's nonlinear variation on the consolidation. The constitutive relationship of the electro-osmotic permeability involves Eq. (8), in which the exponent a is 3.5 based on previous test results. The input for the other variables remains unchanged for the example problems, i.e., element slicing, soil geometry, the electrical resistivities of the pore fluid and the solid particle of soil and the boundary condition.

Table 4: EC1 example problems.

Variable	Value
Length of the soil mass, L (m)	1
Height of the soil mass, H_0 (m)	1
Voltage gradient, i_e (V/m)	10, 20, 30 and 50
Compressibility	Non-linear Eq. (13) C_c=1.0
Hydraulic conductivity, k_h (m/s)	Variable Eq. (3) C_k=1.0
Electro-osmotic permeability, k_e (m^2/s·V)	Variable Eq. (8)
Element, R_j	100
Initial void ratio, e_0	2
Specific gravity, G_s	2.67
Water content, w	75%
Resistivity of the solid particle, ρ_s (Ω·m)	1,000
Resistivity of the pore fluid, ρ_w (Ω·m)	4
Boundary condition	Cathode open and anode closed

5.1 Settlement, degree and efficiency of consolidation

Figure 13 shows the average soil settlement vs. time and the average consolidation degree vs. time curves for the example problems. Along with the increase in the voltage gradient, the settlement of the soil mass increases in rate and value. The soil subjected to a voltage gradient of i_e=50 V/m settles faster than the other three soils. The majority of the settlement occurs over the first 40 days or so. The values of the final settlement increase nonlinearly in response to the increase in the voltage gradient. Given the 1 m high soil mass, the average final settlement is 0.330 m for i_e=50 V/m, 0.278 m for i_e=30 V/m, 0.227 m for i_e=20 V/m and 0.150 m for i_e=10 V/m. According to the trends in Figure 13(a), the rate and the final value of the settlement for i_e>50 V/m are less likely to increase by a large amount.

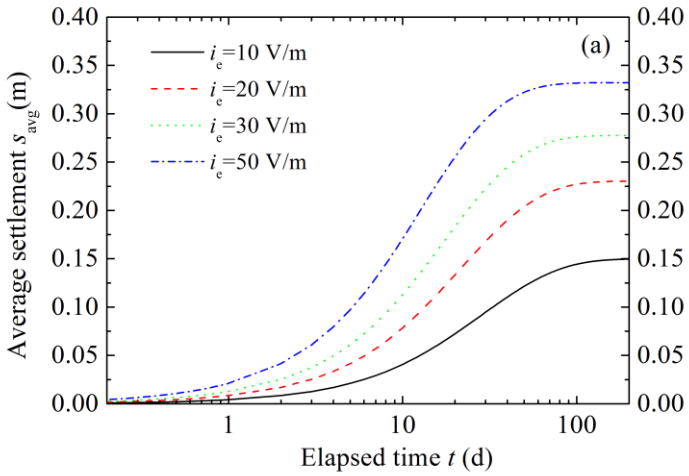

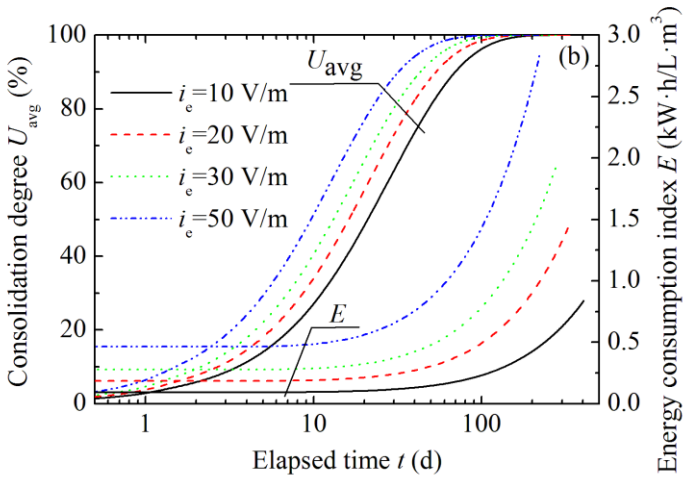

Figure **13**: Example problem: (a) average final settlement vs. time and (b) average consolidation degree vs. time.

Three criteria are often combined to assess the efficiency of electro-osmotic consolidation, i.e., the settlement achieved (equal to the volume of water discharge), the time elapsed and the energy consumed to accomplish the settlement. The aim of practical applications is to consolidate the soil to a sufficiently high extent of settlement given a relatively small elapsed time and energy consumption. The first criterion (water discharge) and third criterion (energy consumption) are combined into an energy consumption index, E, which is the energy consumption (kW·h) per unit volume of soil mass (m^3) and per unit volume of water discharge (liter or L) and is calculated as

$$E = \frac{V_m}{V_v q^{(t_2 - t_1)}} \int_{t_1}^{t_2} I^t \mathrm{d}t \tag{35}$$

where I^t is the variable of the electrical current against time t, V_v is the volume of the soil mass, t_1 and t_2 are, respectively, the start and end time (h) of interest, and $q^{(t_2 - t_1)}$ is the volume of discharge between t_1 and t_2. The unit of the index E is kW· h/L·m^3. The second criterion of the elapsed time is not included because the elapsed time is dependent on the volume of discharge.

The curves of the energy consumption index vs. the elapsed time and the consolidation degree vs. the elapsed time are shown in Figure **13**(b). The lower the voltage gradient is, the lower the energy consumption index, which means that the application of a relatively low voltage between electrodes helps reduce energy consumption when the same amount of water discharge is demanded. Specifically, for the first 10 days, the values of E are 0.09 kW·h/L·m^3 for V_m = 10 V and 0.463 kW·h/L·m^3 for V_m= 50 V. The choice of V_m= 50 V, however, expedites the discharge of water (soil settlement) in contrast to the choice of V_m = 10 V, which increases the amount of elapsed time. From Figure **13**(a), for instance, given the same amount of settlement of 28.4 mm, the elapsed time is 6.83 days for the case of V_m = 10 V and 1.37 days for V_m = 50 V. That is, an electro-osmotic consolidation scenario of applying a relatively higher V_m saves the consolidation time, although the scenario involves a less energy-efficiency index (for the unit discharge of water) and a higher consumption of the total electrical energy (for the full discharge of water). In this circumstance, a compromise between the two factors is needed. As previously mentioned, an electrical gradient of i_e = 30 V/m is a regular choice in practice, which is in agreement with EC1's numerical results.

The energy consumption index, E, basically stays constant and is relatively low at early stage of consolidation (say before the consolidation degree approaches 60% or so), after which the index increases for all choices of a different applied voltage. Taking V_m=30 V for instance, the value of E ranges from 0.27 (t = 0) to 0.30 (t = 17 d) when the consolidation degree U_{avg} increases to 60%. The value of E increases to 0.37 when U_{avg} is 80% at t = 30 d. From elapsed time of 30 d onwards, the value of E climbs up clearly. As an index defined to assess the use of electricity against water discharge volume, E of relatively low value at early stage of consolidation means a favorable use of the electricity, and vice versa. Meanwhile, in the same diagram of Figure 13(b), it is shown that the consolidation degree is largely approaching 90% when the values of E start to increase at a higher gradient. That is, keeping

charging the soil leads to limited consolidation (say less than 10%) while consuming relatively higher electricity. Hence, it is suggested to terminate the electricity when the consolidation completes 90% or around.

The consolidation of the soil is expedited in response to the increase in the voltage gradient. The elapsed times to reach a consolidation degree of 90% are 70 days for a voltage gradient of i_e=10 V/m, 51 days for i_e=20 V/m, 42 days for i_e=30 V/m and 31 days for i_e=50 V/m. That is, the higher the voltage gradient is, the earlier the major settlement is accomplished. Based on the preceding discussion of the energy consumption and elapsed time, the choice of i_e=30 V/m outperforms the other choices for the soil geometry involved in the example problems and is regarded as a cost-effective voltage gradient that offers a satisfactory value of settlement and favorable energy saving.

Figure **14** shows the curves of the average consolidation degree vs. time at three particular positions, i.e., the anode, the center and the cathode for V_m=30 V. Over the first 3 days, a consolidation degree of 35% is reached for the soils adjacent to the anode, whereas no clear consolidation occurs for the soils in the center and adjacent to the cathode. After 3 days, the soils close to the anode continue consolidating substantially, and the soils in the center and around the cathode start to consolidate. Along with the movement of water from the anode toward the cathode, the escape of water from the soils close to the anode results in immediate consolidation as the boundary at the anode is set closed. The escaped water volume flows through the centre and toward the cathode, and tends to replace the portion of water escaped from the soils at the centre and cathode. As a result, the consolidation of soils at the centre and cathode does not immediately occur but lags. From Figure 14, the lag of time is up to 3 days depending upon the position of soils.

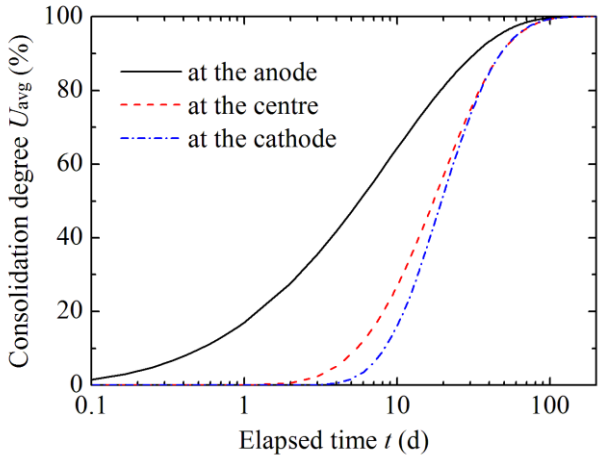

Figure **14**: Example problem: the average consolidation degree vs. time at particular positions.

As consolidation is position dependent, it is of interest to suggest an average cut-off time to account for the accomplishment of major consolidation of the entire soil mass. Based on the time range of the curves in Figure 14, the closer the soils are to the anode, the wider the time range is, and vice versa. That is, the soils around the anode start to consolidate early and progressively increase at relatively low gradient, whereas the consolidation for the soils close to the cathode lags for 3 days and then commences and proceeds drastically at a relatively high gradient. At the end, the curves converge at some time of 100 days, which means soils of different positions cease settling simultaneously. An elapsed time of 60 days is selected as a cut-off point suitable for the entire soil mass, where 95% to 97% consolidation has been accomplished.

5.2 Pore pressure and electrical potential

Figure **15** shows the pore pressure vs. time computed at the center and at the anode of the electro-osmotic geometry as the voltage gradient varies. For the soils of the same position, the higher the voltage gradient i_e is, the higher the peak values are of the pore pressure. At the anode, for instance, the pore pressure reaches up to –315 kPa for i_e=50 V/m

and −50 kPa for i_e=10 V/m. Regarding soils of different positions, the pore pressure is much higher at the anode than at the center. When subjected to an electrical gradient of 50 V/m, for instance, the soils have pore pressure of −315 kPa at the anode and −90 kPa in the center. The pore pressure is likely to dissipate significantly and might not climb up to values of hundreds of kilopascals in practice because soils are rarely exposed to the ideal conditions applied to the model. Nevertheless, high negative pore pressure did lead to cavitations at the anode, cracks and fissures in soils which were observed in tests. The soil cracks and fissures occurred more likely to the soils around the anode than the cathode, which is in agreement with respective pore pressures. And the cracks and fissures extended in soil mass along with the progress of consolidation and development of pore pressures.

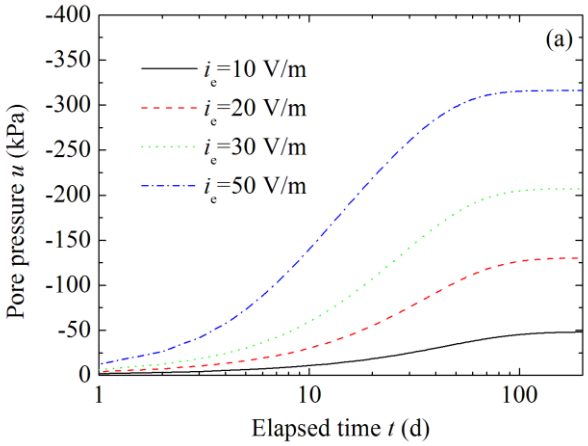

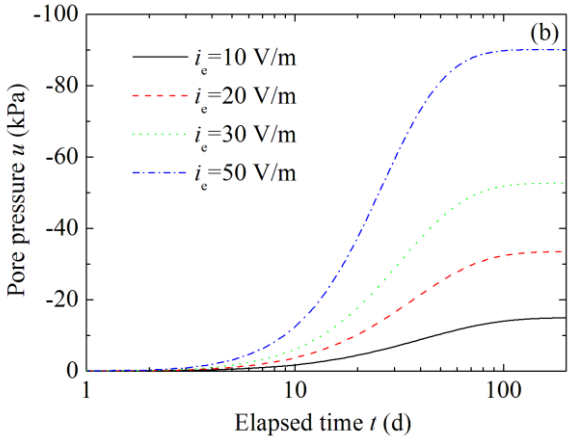

Figure **15**: Example problem: (a) pore pressure at the anode vs. time and (b) pore pressure at the center vs. time.

Figure **16** shows the curves of the pore pressure over time vs. the distance to the cathode and the electrical potential over time vs. the distance to the cathode V_m=30 V. The curves are plotted in a normalized format. The pore pressure at the cathode is zero over the elapsed time because of the boundary of the open cathode. Over the distance toward the anode, the pore pressure increases nonlinearly. Over the elapsed time of consolidation, the pore pressure increases nonlinearly as well, which is similar to the validation results indicated in Figure **5**.

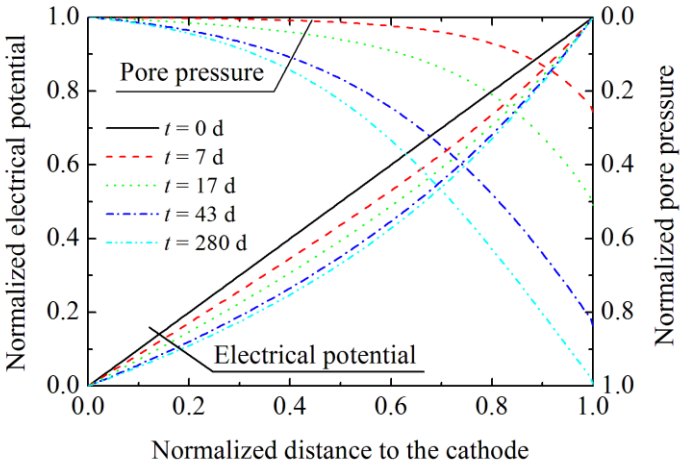

Figure 16: Example problem: (a) the normalized pore pressure vs. the distance to the cathode and (b) the normalized electrical potential vs. the distance to the cathode.

In Figure 16, the form of the electrical potential is similar to that in Figure 11. The potential starts with a linear distribution and then turns into a series of concave curves over time. The slope of the tangent of the curve at a position is indicative of the potential drop at that position. The concave curves lead to the progressive reduction of the slope from the anode toward the cathode. As a result, the electrical potential drops to a higher extent for the soils close to the anode than to the cathode. Specifically, the potential drop becomes sequentially severe when the point of interest approaches the anode. The nonlinear potential drop is associated with the oriented one-dimensional flow of the pore fluid. Along with the flow of fluid toward the cathode, the water content of the soil mass redistributes appropriately so that the soils on the side of the anode become drier and the other side becomes wetter. Consequently, the electrical resistivity of the soil is not uniform but varies with the position. The resistivity decreases nonlinearly from the anode toward the cathode, which results in the nonlinear drop and concave distribution of the electrical potential.

6. CONCLUSIONS

EC1, a one-dimensional large-strain electro-osmotic consolidation model, was developed, validated and implemented. The model, which is in the form of a non-linear finite-difference equation, represents a collection of several constitutive relationships, particularly, the relationships for the compressibility, hydraulic conductivity, electro-osmotic permeability and electrical resistivity in response to a large-strain settlement and as a function of the void ratio. EC1 is validated against analytical exact solutions involving a small-strain settlement. For experimental tests where large-strain settlement occurs, the performance of EC1 is acceptable.

In addition to validating the numerical model, the experimental tests lead to the setups of the hydraulic and electro-osmotic permeameter, the Miller soil box and the electro-osmotic consolidation box. The permeameter is novel in that it provides the measurements of the electro-osmotic permeability as well as the hydraulic conductivity in one domain. The void ratio of the soil placed in the permeameter varies so that the relationship between the electro-osmotic permeability and the void ratio can be found. The Miller box is deployed to determine the relationship between the electrical resistivity and the void ratio, which leads to the approximation of the respective resistivity of the pore fluid and the solid particle of soils. The electro-osmotic consolidation box is designed to imitate a one-dimensional horizontal flow for different boundary conditions. The use of the box successfully implements the electro-osmotic consolidation of soils, allowing the measurements of the electrical potential at various positions and the estimates of the flow rate over time.

Based on the numerical results of the example problems involving one-dimensional large-strain electro-osmotic consolidation, a parametric study was conducted with respect to the consolidation degree, settlement of the soil, rate of flow and pore pressure of the soil. A higher voltage gradient leads to expedited consolidation and increased settlement. The increase in the rate and value are nonlinear in response to the increase in the voltage gradient. An input of voltage gradient 30 V/m is a cost-effective choice and has advantages in terms of the energy need, elapsed time and settlement value compared with the other choices of the electrical gradient. For the choice of 30 V/m, a cut-off point of 43 days is noted, which is when the entire soil mass accomplishes 90% consolidation. The value of 90% for the consolidation degree is also a cut-off point, which is when it is plausible to terminate the energy input for electro-osmosis and avoid substantial waste of energy afterwards. Consolidation commences sequentially from the anode toward the cathode, and eventually, soils of all positions approach the end of consolidation simultaneously. The electro-osmotic

permeability marginally expedites the consolidation of soils under a large-strain deformation. Both the electrical potential and pore pressure develop nonlinearly over time and through the soil mass. The closer the soil is to the anode, the higher the pore pressure is, and the earlier the pore pressure reaches its peak value.

ACKNOWLEDGMENTS

The study began in Hohai University and was continued and completed when the second author moved to the University of Adelaide. The authors appreciate the technical support provided by Hohai University and the EMCS start-up grant of the University of Adelaide. The programming code offered in Fox and Berles's paper[15] was referred to and highly appreciated.

NOTATIONS

a	Experimental derived exponent of the coefficient of electro-osmotic permeability
a_v	Coefficient of compressibility
A_j	Average area of the cross section between contiguous elements, j and (j–1)
C_c	Compression index
C_k	Hydraulic permeability index
D	Dielectric constant of pore fluid
e	Void ratio
e^*	Threshold void ratio
E	Energy consumption index
G_s	Specific gravity of soil solids
h	Total head of water
h_{w1}	Total head of water adjacent to cathode
h_{w2}	Total head of water adjacent to anode
H_0	Initial height of compressible soil mass
i_e	Voltage gradient
i_h	Hydraulic gradient
j	Element co-ordinate
k	Coefficient of hydraulic or electro-osmotic permeability
k_e	Coefficient of electro-osmotic permeability

744	k_{es}	Equivalent series coefficient of electro-osmotic permeability
745	k_h	Coefficient of hydraulic permeability
746	k_{hs}	Equivalent series coefficient of hydraulic permeability
747	k^*	Threshold coefficient of permeability
748	l_0	Thickness of element
749	L	Length of compressible soil mass
750	m	Loop calculation termination variable
751	n	soil porosity
752	p	stress/load in oedometer test
753	q	Volume of flow
754	q_h	Flow volume induced by hydraulic gradient
755	q_e	Flow volume induced by electrical gradient
756	R_j	Number of elements for soil mass
757	R_m	Number of piece-linear points in compressibility constitutive relationship curves
758	R_n	Number of piece-linear points in permeability constitutive relationship curves
759	s_{avg}	Average settlement of soil mass
760	s_j	Settlement of element j
761	t	Elapsed time of consolidation
762	t_f	Final elapsed time
763	T_v	Time factor
764	u	Pore pressure
765	U_{avg}	Average consolidation degree
766	V_j	Electrical potential at element j
767	V_m	Electrical potential difference between electrodes
768	V_v	Volume of soil mass
769	w	Water content
770	w_p	Plastic limit
771	w_L	Liquid limit
772	W	Width of compressible soil mass
773	x	Distance from cathode to anode
774	$z_{c,j}$	Elevation of upper corner of element j
775	z_j	Elevation of node of element j
776	σ	Total stress
777	σ'	Effective stress
778	η	Viscosity of t pore fluid
779	γ	Unit weight of soil
780	γ_w	Unit weight of water
781	ξ	soil zeta potential

ρ	Electrical resistivity
ρ_s	Electrical resistivity of soil solid particles
ρ_w	Electrical resistivity of pore water

REFERENCES

1. Casagrande, L., *Electro-Osmosis in Soils.* Géotechnique, 1949. **1**(3): p. 159-177.
2. Win, B.M., V. Choa, and X.Q. Zeng, *Laboratory investigation on electro-osmosis properties of Singapore marine clay.* Soils and Foundations, 2001. **41**(5): p. 15-23.
3. Mesri, G. and R.E. Olson, *Mechanisms controlling permeability of clays.* Clays and Clay Minerals, 1971. **19**(3): p. 151-&.
4. Shuang, J.Q. and K.S. Ho, *Electro-osmotic consolidation behaviour of two Ontario clays.* Geotechnical Engineering for Disaster Mitigation and Rehabilitation, 1998. **29**(2): p. 181-194.
5. Esrig, M.I., *Pore pressure, consolidation and electrokinetics.* J. Soil Mech. Found. Div., 1968. **94**(SM4): p. 899-922.
6. Wan, T.Y. and J.K. Mitchell, *Electro-osmotic consolidation of soils.* J. Geotech. Eng. Div., 1976. **102**(5): p. 473-491.
7. Su, J.Q. and Z. Wang, *The two-dimensional consolidation theory of electro-osmosis.* Geotechnique, 2003. **53**(8): p. 759-763.
8. Gibson, R.E., G.L. England, and M.J.L. Hussey, *Theory of 1-dimensional consolidation of saturated clays .1. finite non-linear consolidation of thin homogeneous layers.* Geotechnique, 1967. **17**(3): p. 261-&.
9. Feldkamp, J.R., *Numerical-analysis of one-dimensional nonlinear large-strain consolidation by the finite-element method.* Transport in Porous Media, 1989. **4**(3): p. 239-257.
10. Feldkamp, J.R. and G.M. Belhomme, *Large-strain electrokinetic consolidation - theory and experiment in one dimension.* Geotechnique, 1990. **40**(4): p. 557-568.
11. Townsend, F.C. and M.C. Mcvay, *SOA: Large Strain Consolidation Predictions.* Journal of Geotechnical Engineering-ASCE, 1990. **116**(2): p. 222-243.
12. Olson, R.E. and C.C. Ladd, *One-dimensional consolidation problems.* J. Geotech. Eng. Div. ASCE, 1979. **105**: p. 11-30.
13. Yong, R.N., S.K.H. Siu, and D.E. Sheeran, *On the stability and settling of suspended solids in settling ponds. Part I. Piece-wise linear consolidation consolidation analysis of sediment layer.* Canadian Geotech J, 1983. **20**: p. 817-826.
14. Yong, R.N. and C.A. Ludwig, *Large-strain consolidation modelling of land subsidence*, in *Proc. Symp. on Geotechnical Aspects of Mass and Materials Transport*. 1984: Bangkok, Thailand. p. 14-29.
15. Fox, P.J. and J.D. Berles, *CS2: A piecewise-linear model for large strain consolidation.* International Journal for Numerical and Analytical Methods in Geomechanics, 1997. **21**(7): p. 453-475.
16. McVay, M., F. Townsend, and D. Bloomquist, *Quiescent consolidation of phosphatic waste clays.* J. Geotech. Eng. ASCE, 1986. **112**: p. 1033-1049.
17. Deng, A. and Y. Zhou, *A piecewise-linear numerical model for one-dimensional electroosmosis consolidation*, in *The Proceedings of International Conference on Ground Improvement (ICGI 2012)*. 2012: Wollongong. p. 1369-1375.

18. Shang, J.Q., *Electroosmosis-enhanced preloading consolidation via vertical drains.* Canadian Geotechnical Journal, 1998. **35**(3): p. 491-499.
19. Lo, K.Y., K.S. Ho, and I.I. Inculet, *Field-Test of Electroosmotic Strengthening of Soft Sensitive Clay.* Canadian Geotechnical Journal, 1991. **28**(1): p. 74-83.
20. Jeyakanthan, V., C.T. Gnanendran, and S.C.R. Lo, *Laboratory assessment of electro-osmotic stabilization of soft clay.* Canadian Geotechnical Journal, 2011. **48**(12): p. 1788-1802.
21. Lo, K.Y., I.I. Inculet, and K.S. Ho, *Electroosmotic Strengthening of Soft Sensitive Clays.* Canadian Geotechnical Journal, 1991. **28**(1): p. 62-73.
22. Taylor, D.W., *Fundamentals of Soil Mechanics*. 1948, New York: John Wiley & Sons, Inc.
23. Carrier, W.D., L.G. Bromwell, and F. Somogyi, *Design capacity of slurried mineral waste ponds.* J. Geotech. Engng Div. ASCE, 1983. **109**(699-716).
24. Fox, P.J., *Solution charts for finite strain consolidation of normally consolidated clays.* Journal of Geotechnical and Geoenvironmental Engineering, 1999. **125**(10): p. 847-867.
25. Mitchell, J.K. and K. Soga, *Fundamentals of Soil Behavior*. 2005: John Wiley & Sons, Inc.
26. Bowen, W.R. and P.M. Jacobs, *Electroosmosis and the Determination of Zeta-Potential - the Effect of Particle Concentration.* Journal of Colloid and Interface Science, 1986. **111**(1): p. 223-229.
27. Turner, J.C.R., *2-phase conductivity - electrical conductance of liquid-fluidized beds of spheres.* Chemical Engineering Science, 1976. **31**(6): p. 487-492.
28. Fricke, H., *The electric conductivity of disperse systems.* Journal of General Physiology, 1924. **6**(6): p. 741-746.
29. Fricke, H., *A mathematical treatment of the electrical conductivity of colloids and cell suspensions.* Journal of General Physiology, 1924. **6**(4): p. 375-384.
30. Komine, H., *Estimation of chemical grouted soil by electrical resistivity.* Ground Improv, 1997. **1**(2): p. 101-113.
31. Gray, D.H. and J.K. Mitchell, *Fundamental aspects of electro-osmosis in soils.* J. Soil Mech. Found. Div., 1967. **93**(SM6): p. 209-236.
32. Deng, A. and M. Zhang, *A consolidation model of single drain driven by combining vacuum preloading and electroosmosis*, in *Geosynthetics Asia 2012*, D.T. Bergado, Editor. 2012: Bangkok. p. 191-200.
33. Yukselen-Aksoy, Y. and K.R. Reddy, *Electrokinetic delivery and activation of persulfate for oxidation of PCBs in clayey soils.* Journal of Geotechnical and Geoenvironmental Engineering, 2013. **139**(1): p. 175-184.
34. Al-Hamdan, A.Z. and K.R. Reddy, *Electrokinetic remediation modeling incorporating geochemical effects.* Journal of Geotechnical and Geoenvironmental Engineering, 2008. **134**(1): p. 91-105.
35. Mohamedelhassan, E. and J. Q. Shang. *Effects of electrode materials and current intermittence in electro-osmosis*. Ground Improvement, 2001, **5**(1): 3-11.
36. Carter, J.P., J.C. Small and J.R. Booker. *A theory of finite elastic consolidation*. International Journal of Solids and Structures, 1977, **13**(5): 467-478.
37. Cargill, K.W. *Prediction of consolidation of very soft clay*. Journal of Geotechnical Engineering, 1984, **110**(6): 775-795.
38. Chen, J.L. and L. Murdoch, *Effects of electroosmosis on natural soil: Field test.* Journal of Geotechnical and Geoenvironmental Engineering, 1999. **125**(12): p. 1090-1098.